# Nearshore Bathymetry From Fusion of Sentinel-2 and ICESat-2 Observations

Andrea Albright<sup>©</sup> and Craig Glennie<sup>©</sup>, Member, IEEE

Abstract—Nearshore estimates of bathymetry are crucial for understanding coastal processes. However, current passive remote sensing methods for estimating bathymetry require in situ depth measurements to train inversion models, which can be difficult or impossible to obtain in many areas. To address this issue, we investigated the fusion of range measurements from the advanced topographic laser altimeter system (ATLAS) aboard the NASA ICESat-2 satellite, and multispectral satellite imagery from European Space Agency (ESA) Sentinel-2 using two common bathymetric inversion algorithms. The active ranging capability of the ATLAS green (532-nm) laser has been shown to generate returns of up to 38-m depth in optically clear waters, providing depth measurements to constrain passive bathymetric inversion results. Data acquired in November 2018 over the nearshore in Destin, FL, USA, offer a proof of concept for this approach. The results of the bathymetric inversion were quantitatively assessed by comparison with airborne bathymetric LiDAR collected using the U.S. Army Corps Coastal Zone Mapping and Imaging LiDAR (CZMIL) system in October-November 2018. Overall, the results of the bathymetric inversion compared with the CZMIL data have a root mean square error (RMSE) of 0.35 m in waters with similar turbidity and bottom reflectivity, and demonstrate that a combination of ICESat-2 depth observations with Sentinel-2 multispectral imagery can estimate seamless nearshore bathymetry for optically clear coastal waters.

Index Terms—Bathymetry, ICESat-2, Sentinel-2, support vector regression (SVR).

# I. INTRODUCTION

THERE is currently a global lack of bathymetric data covering the shallow nearshore zone, extending seaward from the shoreline to the 5–10-m depth contour [1]. Even in developed countries with well-funded hydrographic surveying offices, data are frequently lacking in the shallowest areas, and in remote coastal regions, there is almost no available data [2]. The most viable techniques for mapping coastal (generally, <30 m depth) bathymetry are using conventional acoustic methods or airborne LiDAR bathymetry (ALB). Sonar, which is boat-based, is difficult and dangerous to deploy in the nearshore (i.e., near rocks, reefs, and in areas of significant

Manuscript received October 1, 2019; revised February 3, 2020; accepted April 3, 2020. The work of Andrea Albright was supported by the National Defense Science and Engineering Graduate (NDSEG). The work of Craig Glennie was supported by the National Science Foundation Instrumentation and Facility under Grant #1830734. (Corresponding author: Andrea Albright.)

The authors are with the Department of Civil and Environmental Engineering, University of Houston, Houston, TX 77386 USA (e-mail: aabright@uh.edu; clglennie@uh.edu).

This article has supplementary downloadable material available at http://ieeexplore.ieee.org, provided by the authors.

Color versions of one or more of the figures in this letter are available online at http://ieeexplore.ieee.org.

Digital Object Identifier 10.1109/LGRS.2020.2987778

wave action). ALB is difficult to deploy in remote areas, and requires significant human and monetary resources for acquisition. As a result, neither method is viable for repeated global acquisition of high-resolution nearshore bathymetry. For better understanding of coastal processes, a more continuous and seamless estimate of nearshore bathymetry is desirable [3], [4]. Spectral-based approaches for water depth estimation using multi and hyperspectral imagery have been well established in the published literature going back more than four decades [5]. Although there is an empirical relationship between light attenuation and water depth [6], complex factors, such as primary production, turbidity, and bottom-type, can further complicate the nonlinear relationship between surface reflectance and water depth in ways that cannot be empirically determined [7]. Consequently, in situ depths are required to calibrate spectral-based approaches to achieve reasonable accuracy. While in situ depths are not currently available on a global scale, the recent launch of ICESat-2 equipped with a green laser profiler capable of shallow water bathymetry has the potential to unlock this possibility. This is the first study, to our knowledge, that uses ICESat-2 determined water depths to seed bathymetric inversion models.

Previous studies using NASA's airborne photon-counting ICESat-2 simulator, Multiple Altimeter Beam Experimental Lidar (MABEL), suggest that measuring bathymetry from ICESat-2 is possible [8], [9], but it has been an open question if those results can be duplicated using range profiles from ICESat-2. Even if bathymetric measurements were possible, the spacing between beam pairs is wide enough -3 km at low latitudes—that ICESat-2 alone would be insufficient for compiling high-resolution bathymetric models. However, depths measured from ICESat-2 profiles could be used to seed satellite derived bathymetry (SDB). A recent publication presents first evidence that ICESat-2 can measure water depths of up to 38 m in optically clear waters [10]. This letter leverages these initial findings to investigate the fusion of ICESat-2 depth profiles with multispectral satellite imagery from Sentinel-2. Using ICESat-2 profiles and Sentinel-2 imagery collected over Destin, FL, USA, in November 2018, we present a comparison of linear regression (LR) and machine learning support vector regression (SVR) bathymetric inversion algorithms for deriving seamless high-resolution nearshore bathymetry. We demonstrate that using these techniques, seamless bathymetric maps can be obtained with a mean difference of 0.01 m  $\pm$  0.35 m (mean  $\pm$  std.), root mean square error (RMSE) = 0.35 m between the model and the independent ground truth provided by coincident ALB observations (negative difference indicates reference is shallower than the model).

1545-598X © 2020 IEEE. Personal use is permitted, but republication/redistribution requires IEEE permission. See https://www.ieee.org/publications/rights/index.html for more information.

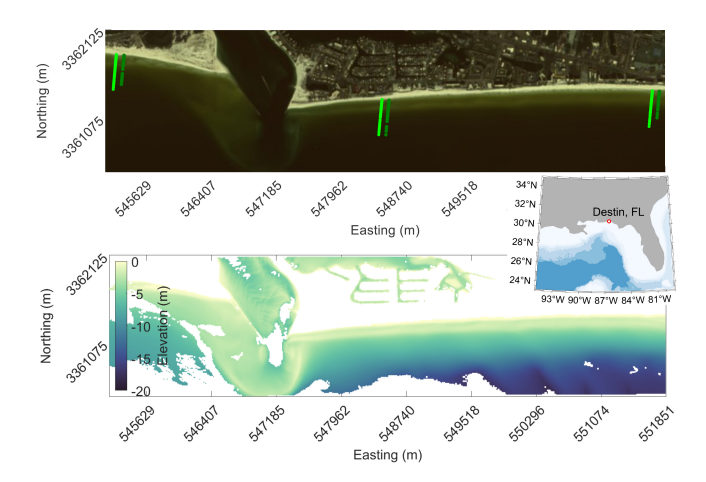


Fig. 1. (Top) Sentinel-2 image RGB composite collected on November 16, 2018, ICESat-2 depth profiles collected on November 18, 2018, strong beams (west, light green), weak beams (east, dark green), beam pairs numbered 1–3 from east to west; (Bottom) USACE CZMIL topobathymetric LiDAR collected October–November 2018. Elevation ranges from 0.4 to -18.7 m and is reported as orthometric NAVD 88 heights using GEOID12B.

#### II. METHODS

## A. Study Site

The site is located around the East Pass near Destin, FL, USA-a tidal inlet that connects the Gulf of Mexico with the Choctawhatchee Bay (Fig. 1). The inlet is bounded by jetties constructed by the U.S. Army Corps of Engineers (USACE), who also regularly dredge the channel, which adds a man-made element to this study area. Water depths vary from 0 m to greater than 18 m, and the optical clarity of the water makes it ideal for measuring the performance of ICESat-2 bathymetric profiles. The beach is oriented in the east/west direction such that the near polar orbit of ICESat-2 is perpendicular to beach, which is optimal for collecting a profile with the widest range of water depths. In addition, this location is coincident with an airborne bathymetric LiDAR data set collected in 2018 by the USACE Optech Coastal Zone Mapping and Imaging LiDAR (CZMIL) system used here for independent validation.

## B. Observations

1) ICESat-2: Launched in September 2018, the advanced topographic laser altimeter system (ATLAS) aboard the NASA satellite ICESat-2 uses a 532 nm laser with a 17 m footprint to detect the elevation of land and water surfaces on a global scale [11]. The laser can operate at a high repetition rate, 10 kHz, which results in 70 cm separation for each laser shot in the alongtrack direction [8]. A diffractive optical element splits the laser into six beams, three pairs of strong and weak beams spaced 90 m apart, and 3 km spacing between pairs of beams, which provides increased spatial coverage [12]. On November 18, 2018, ICESat-2 orbited over East Pass on a descending track. Of the three beam pairs, one pair landed to the west of the pass and two pairs are located eastward (Fig. 1).

The L2A Global Geolocated Photon Data (ATL03) contain noise common to single photon counting LiDAR systems,

primarily solar noise and atmospheric scattering [13]. Existing filtering algorithms and higher level data products have not been optimized for bathymetric applications [14], [15], and therefore, classification of points was done manually.

2) Sentinel-2: Multispectral Sentinel-2 imagery [16] was used for bathymetric inversion in this letter. The image used here is a Level-2A image collected on November 16, 2018, which is an orthoimage, bottom of the atmosphere corrected reflectance product. Only the 10 m resolution bands were used, namely bands B2 (Blue/497 nm), B3 (Green/560 nm), B4 (Red/665 nm), and B8 (NIR/835 nm). A normalized difference vegetative index (NDVI) was applied to mask out nonwater pixels using a threshold of -0.2

Nonwater Pixels = 
$$\frac{B8 - B4}{B8 + B4} > -0.2$$

3) USACE CZMIL: The airborne LiDAR data set was collected after Hurricane Michael from October 24–November 04, 2018 by the Joint Airborne LiDAR Bathymetry Technical Center of eXpertise (JALBTCX) CZMIL system of the USACE [17]. The LiDAR system collects data at 10 kHz with a planned data density of at least 2 points/m² in shallow water, 0.5 points/m² in deep water, and classified bathymetric point clouds that meet the standard of 3.5 + 0.05d m horizontal accuracy and  $((0.30^2) + ((0.013d)^2))^{1/2}$  m vertical accuracy at 95% confidence level, where d is depth. CZMIL data are provided in a presegmented format with benthic layer returns already identified for easy bathymetry retrieval and these returns were used to generate the bathymetric map in Fig. 1.

## C. Data Processing

1) Index of Refraction Correction: The ATLAS/ ICESat-2 L2A Global Geolocated Photon Data Product (ATL03) [18] assumes that the photons collected have traveled primarily through air, but for bathymetric points the photons must also travel through water slowing the return of the incident photon. When light crosses the air-sea barrier, the phase velocity decreases due to the change in propagation medium. The index of refraction (n) change results in points that are measured deeper than would be expected based on a time-of-flight calculation through air, and points that are horizontally offset due to slant range from a nonzero angle of incidence in the case of nonnadir facing lasers (four laser beams are nonnadir). A rigorous explanation of the necessary corrections, including accounting for the curvature of the Earth across the swath, is given in [10]. In this letter, a correction is applied to the water depths measured to account for the index of refraction in seawater (T = 20 °C, S = 33 practical salinity units (PSU), at atmospheric pressure,  $\lambda = 546.1 \text{ nm}, n = 1.324)$  [6]. Parrish *et al.* [10] points out that the widest angle of incidence is currently 0.38°, which corresponds to a horizontal offset refraction correction of 0.003d, where d is depth, or <4 cm at 12-m water depth. The horizontal refraction correction was deemed negligible in comparison to the beam footprint (17 m) and a vertical correction was applied.

- 2) Datum Transformation: ICESat-2 photons are reported as geographical coordinates using the World Geodetic System 1984 (WGS84) ellipsoid in the ITRF2014 reference frame, and the USACE/CZMIL points are reported as geographical coordinates in the North American Datum of 1983 (NAD83) with the vertical elevations referenced to the North American Vertical Datum of 1988 (NAVD 88) using geoid model GEOID12B. ICESat-2 photons were transformed into the NAD83 datum and ellipsoid heights were converted to orthometric heights, and all points were projected into Universal Transverse Mercator (UTM) 16N using National Oceanic and Atmospheric Administration (NOAA)'s VDatum software.
- 3) Bathymetric Inversion: The use of bathymetric inversion models requires a training data set to tune the model for optimal performance. For our experiments, depth measurements are provided by the ICESat-2 refraction corrected range measurements [19] and then their respective locations are matched via their coordinates to corresponding Sentinel-2 pixels to build a training data set. For comparative purposes, we trained two algorithms to model bathymetry at each pixel location. The first inversion model is a linear transform model [5] and the second is a nonlinear machine learning technique named SVR [20].
- a) LR: There is a long history of applying a simple linear model to correlate surface reflectance recorded in satellite image pixels with depth. First developed by Lyzenga [5], [21] this method requires relatively little computational effort and can be expanded to accommodate any number of wavelength bands. The downside is that it assumes homogeneous water quality and bottom type throughout the scene and that the nonlinear relationship between surface reflectance and depth can be adequately modeled using a polynomial function of n+1 tunable parameters  $(a_i)$ , where n is the number of wavelength bands for a given image and  $X_i$  are the min–max normalized reflectance values for each band. This method is widely used in the literature [22], [23] and thus serves as a point of reference for comparison purposes.

$$K = a_0 + \sum_{i=1}^{n} a_i X_i \tag{1}$$

b) SVR: This technique is a machine learning algorithm that uses a training data set to learn the nonlinear relationship between surface reflectance and water depth without any empirical knowledge of the processes that would affect surface reflectance, such as attenuation, turbidity, or bottom type. The support vectors used for regression are found by splitting the known pixel depths (both weak and strong beam returns) 80/20 into uniformly distributed training/validation data sets and mapping the training data set into a multidimensional feature space. The best regression fit is found by using a kernel function and tuning the model parameters to best match the validation data set [24]. Radial basis kernel functions (RBFs) have been shown to model nonlinear behavior with a smaller number of inputs and therefore, work well in this context [20]

$$K(x_i, x_j) = \exp(-\gamma ||x_i - x_j||^2), \quad \gamma > 0.$$
 (2)

The RBF kernel function above has a tunable gamma parameter. Vapnik [25] introduced an error (loss) function

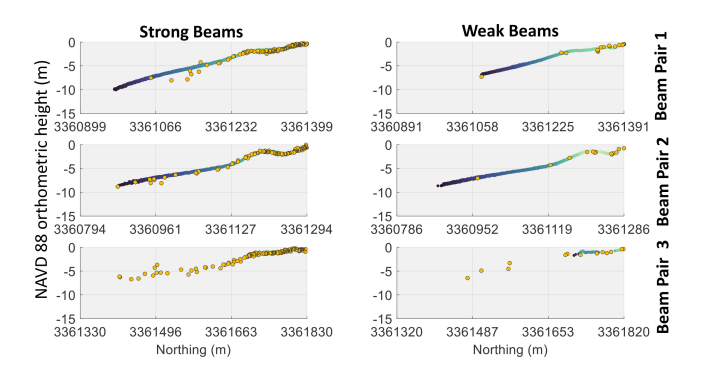


Fig. 2. ICESat-2 points (yellow) overlaid on top of USACE CZMIL points < 1.5 m distance, separated by beam pair into strong and weak profiles.

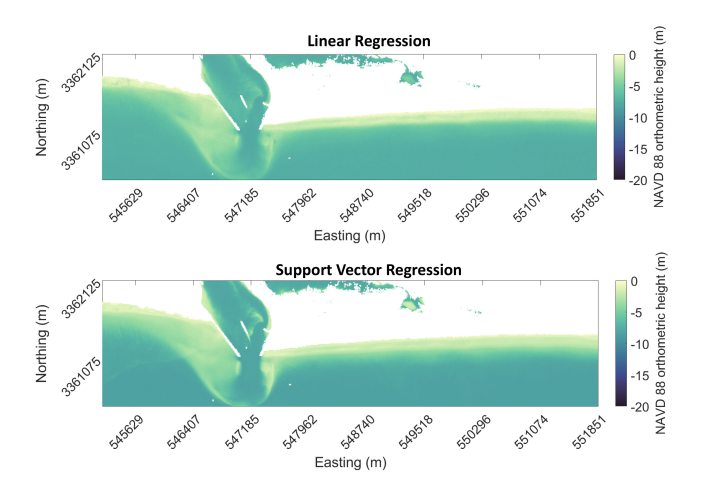


Fig. 3. (Top) LR results range from 1.9 to  $-8.9~\mathrm{m}.$  (Bottom) SVR results range from -0.3 to  $-8.6~\mathrm{m}.$ 

with  $\epsilon$ -insensitivity zone that decreases the number of support vectors, and a cost (C) parameter that decreases the weight of points outside of the  $\epsilon$ -insensitivity zone thereby preventing overfitting. Parameter optimization for these three parameters ( $\gamma$ ,  $\epsilon$ , C) determines the model with the best SVR performance. More details of the use of SVR for bathymetric inversion can be found in [20]. LIBSVM software was used to create the SVR model used in this letter [26].

## III. RESULTS AND DISCUSSION

Profiles collected over Destin, FL, USA, clearly demonstrate the ability of ICESat-2 to capture the shallow water coastline with elevations measured between 0.0 and -8.8 m. The coherence is close between points collected by ICESat-2 and the CZMIL LiDAR (Fig. 2). The RMSE of the profiles ranges from 0.26 to 0.34 m for the strong beams and 0.20–0.31 m for the weak beams, which smaller than the RMSE range of 0.43–0.60 m and 0.43–0.56 m for strong and weak beams, respectively, reported by Parrish *et al.* [10]. In general, the strong beams have  $4\times$  more points than the weak beams. Differences between the strong and weak beams are summarized in Table I. The 95th percentile elevation listed in the table represents the range (from 0) containing 95% of the measured points.

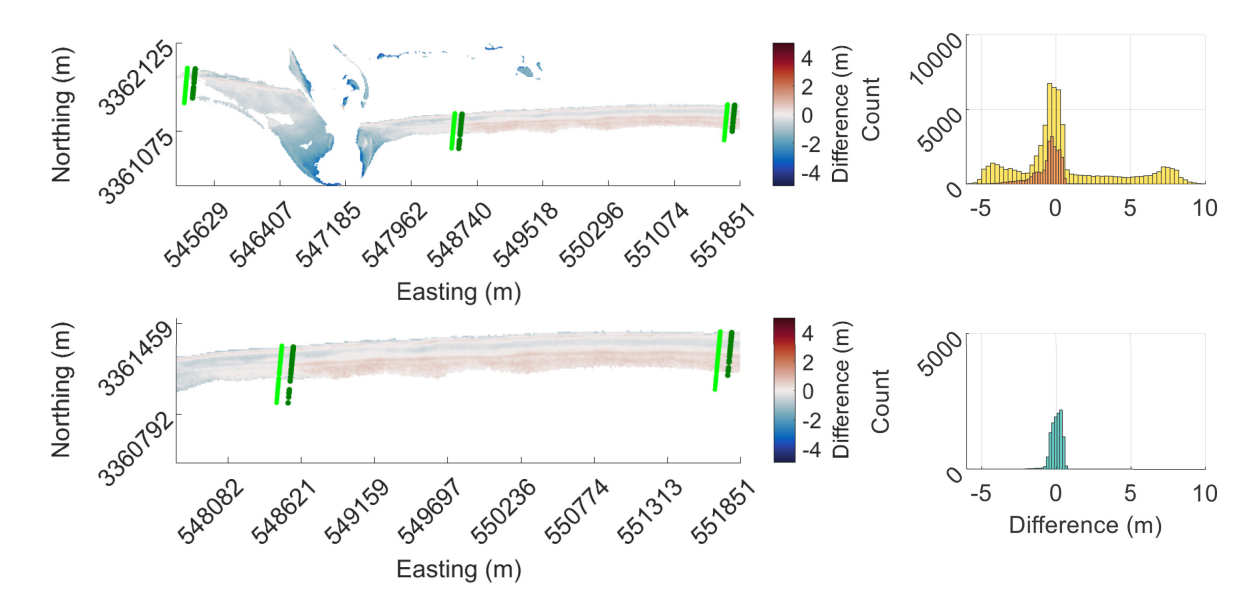


Fig. 4. (Top Left) Error map [IS2/S2-CZMIL]—95th Percentile. (Top Right) Histogram of All Areas (yellow), 95th Percentile (orange). (Bottom Left) Error map [IS2/S2-CZMIL]—95th Percentile between beams 1 and 2. (Bottom Right) Histogram 95th Percentile between beams 1 and 2 (green)—For error maps: blue indicates the model is deeper than reference, red indicates the model is shallower than reference.

TABLE I

COMPARISON OF DIFFERENCE BETWEEN ICESAT-2 PROFILES
AND CZMIL TOPOBATHYMETRIC LIDAR FOR
STRONG AND WEAK BEAMS 1–3

Difference (m)	Strong Beams	Weak Beams
Minimum	-1.26	-0.74
Maximum	0.68	0.46
Mean	-0.11	-0.10
Std. Dev.	0.30	0.26
RMSE	0.32	0.27
# of Profile Points	498	124
95th Percentile Elevation (m)	-6.04	-6.71

TABLE II

COMPARISON OF DIFFERENCE BETWEEN ICES AT-2/
SENTINEL-2 BATHYMETRY AND CZMIL
TOPOBATHYMETRIC LIDAR FOR LR AND
SVR ALGORITHMS

Difference (m)	Linear Regression	Support Vector Regression
Minimum	-9.21	-7.59
Maximum	11.01	9.92
Mean	0.92	0.55
Std. Dev.	3.58	3.32
RMSE	3.70	3.36

The estimated depth maps from the two bathymetric algorithms are presented in Fig. 3. The LR algorithm has a model RMSE = 0.69 m and  $R^2 = 0.93$ , and does not perform as well as the SVR algorithm, model RMSE = 0.14 m and  $R^2 = 0.996$ . Note that these model fits are with respect to the regression validation data, not the CZMIL bathymetry. The SVR algorithm is better able to capture the fine scale features and interpolate for the remaining pixels in the image. The results of the statistical comparison of each technique with the USACE CZMIL data set are summarized in Table II. We conclude based on both the model validation and the external validation data set that SVR is the superior inversion technique. Therefore, further analysis will only be performed on the SVR bathymetry results.

First results indicate that extrapolating the inversion model to depths beyond those measured by ICESat-2 leads to gross inaccuracies when compared to CZMIL LiDAR. In addition, there are outlier ICESat-2 depths that may skew inversion results. To be conservative, we therefore, removed all points beyond the 95th percentile elevation and removed results

where the estimated elevation is deeper than the 95th percentile elevation. When the outlier depths are removed, ICESat-2 profiles are reliably able to measure elevations from 0.0 to -6.0 m and -0.4 to -6.7 m for strong and weak beams, respectively.

It is noteworthy that the area inside east pass is not sampled by the ICESat-2 profiles and the bottom-type seems to be sufficiently different from the natural sandy beaches, probably due to repeated dredging. Depths in this area were consistently underestimated by the SVR model results (Fig. 4). There is also a patchy area in the CZMIL data set around beam 3 (west beam) that made direct comparison in this area difficult. When the error analysis was constrained to the area between beams 1 and 2, then the mean error decreases from  $-0.53 \text{ m} \pm 0.88 \text{ m}$ to 0.01 m  $\pm$  0.35 m and decreases the RMSE from 1.03 to 0.35 m (Table III). These results indicate that the SVR fusion technique works very well in areas that are directly observed by ICESat-2, but in areas deeper than observed by ICESat-2 or areas where bottom types are not sampled directly it will be difficult to accurately estimate bathymetry. Therefore, this approach is best suited for shorelines with homogeneous benthic conditions between ICESat-2 profiles.

TABLE III

STATISTICAL COMPARISON OF SVR BATHYMETRY COMPARISON WITH THE CZMIL LIDAR BATHYMETRY ELEVATIONS WITH 95TH PERCENTILE OF ICESAT-2 DEPTHS, BOTH INCLUDED AND EXCLUDED

Difference (m)	All Areas	95th Percentile	Area Between Beams 1-2
Minimum	-7.59	-5.35	-2.02
Maximum	9.92	5.03	5.03
Mean	0.55	-0.53	0.01
Std. Dev.	3.32	0.88	0.35
RMSE	3.36	1.03	0.35

### IV. CONCLUSION

This letter has further validated that the ICESat-2 ATLAS sensor is able to estimate shallow water bathymetry in nonturbid waters. A comparison with a coincident LiDAR data set established that ATLAS was able to estimate bathymetry with an RMSE range of 0.26-0.34 m and 0.20-0.31 m for strong and weak beams, respectively, over a range of elevations from 0.0 to -8.8 m. The depths were combined with two model-based bathymetric inversion approaches, LR, and SVR. Overall, SVR outperformed the LR technique, the algorithm validation (using only ICESat-2 data points) reported a model RMSE = 0.14 m,  $R^2 = 0.996$  and model RMSE = 0.69 m,  $R^2 = 0.93$ , respectively. The SVR algorithm when trained with the ICESat-2 profiles accurately estimated depth using ATLAS range measurements, and when validated externally with airborne LiDAR, the areas between beams 1 and 2 had a mean difference of 0.01 m  $\pm$  0.35 m and RMSE = 0.35 m. The resultant depth map showed no significant decrease in accuracy between beam profiles 1 and 2, suggesting that if turbidity and bottom reflectance are consistent between profiles, then an SVR combination of ICESat-2 depths and Sentinel-2 spectral observations should be able to provide temporal estimates of near-shore bathymetry with a 91-day repeat rate: the nominal revisit rate of ICESat-2.

#### ACKNOWLEDGMENT

The authors would like to thank Dr. Zhigang Pan and the researchers at the National Center for Airborne Laser Mapping (NCALM): Dr. Fernandez-Diaz, A. Singhania, and D. Hauser. Thanks also to the University of Washington Applied Physics Laboratory for hosting an ICESat-2 workshop, and to three anonymous reviewers whose constructive criticisms have improved this letter.

#### REFERENCES

- [1] N. A. Forfinski-Sarkozi and C. E. Parrish, "Active-passive spaceborne data fusion for mapping nearshore bathymetry," *Photogramm. Eng. Remote Sens.*, vol. 85, no. 4, pp. 281–295, Apr. 2019.
- [2] J. X. Leon, S. R. Phinn, S. Hamylton, and M. I. Saunders, "Filling the white Ribbon a multisource seamless digital elevation model for lizard island, northern great barrier reef," *Int. J. Remote Sens.*, vol. 34, no. 18, pp. 6337–6354, Sep. 2013.
- [3] R. Holman and M. C. Haller, "Remote sensing of the nearshore," Annu. Rev. Marine Sci., vol. 5, pp. 95–113, Jan. 2013.

- [4] D. Traganos, D. Poursanidis, B. Aggarwal, N. Chrysoulakis, and P. Reinartz, "Estimating satellite-derived bathymetry (SDB) with the Google Earth engine and sentinel-2," *Remote Sens.*, vol. 10, no. 6, p. 859, 2018.
- [5] D. R. Lyzenga, "Passive remote sensing techniques for mapping water depth and bottom features," *Appl. Opt.*, vol. 17, no. 3, pp. 379–383, Feb. 1978.
- [6] C. D. Mobley, Light and Water: Radiative Transfer in Natural Waters, New York, NY, USA: Academic, 1994.
- [7] W. D. Philpot, "Bathymetric mapping with passive multispectral imagery," *Appl. Opt.*, vol. 28, no. 8, p. 1569, Apr. 1989.
- [8] M. McGill, T. Markus, V. S. Scott, and T. Neumann, "The multiple altimeter beam experimental lidar (MABEL): An airborne simulator for the ICESat-2 mission," *J. Atmos. Ocean. Technol.*, vol. 30, no. 2, pp. 345–352, Feb. 2013.
- [9] Ñ. Forfinski-Sarkozi and C. Parrish, "Analysis of MABEL bathymetry in keweenaw bay and implications for ICESat-2 ATLAS," *Remote Sens.*, vol. 8, no. 9, p. 772, 2016.
- [10] C. E. Parrish, L. A. Magruder, A. L. Neuenschwander, N. Forfinski-Sarkozi, M. Alonzo, and M. Jasinski, "Validation of ICESat-2 ATLAS bathymetry and analysis of ATLAS's bathymetric mapping performance," *Remote Sens.*, vol. 11, no. 14, p. 1634, 2019.
- [11] W. Abdalati *et al.*, "The ICESat-2 laser altimetry mission," *Proc. IEEE*, vol. 98, no. 5, pp. 735–751, May 2010.
  [12] T. Markus *et al.*, "The ice, cloud, and land elevation Satellite-2 (ICESat-
- [12] T. Markus et al., "The ice, cloud, and land elevation Satellite-2 (ICESat-2): Science requirements, concept, and implementation," Remote Sens. Environ., vol. 190, pp. 260–273, Mar. 2017.
- [13] U. C. Herzfeld et al., "Algorithm for detection of ground and canopy cover in micropulse photon-counting lidar altimeter data in preparation for the ICESat-2 mission," *IEEE Trans. Geosci. Remote Sens.*, vol. 52, no. 4, pp. 2109–2125, Apr. 2014.
- [14] B. Smith et al., "Land ice height-retrieval algorithm for NASA's ICESat-2 photon-counting laser altimeter," Remote Sens. Environ., vol. 233, Nov. 2019, Art. no. 111352.
- [15] N. F. Glenn et al., "Landsat 8 and ICESat-2: Performance and potential synergies for quantifying dryland ecosystem vegetation cover and biomass," Remote Sens. Environ., vol. 185, pp. 233–242, Nov. 2016.
- [16] M. Drusch et al., "Sentinel-2: ESA's optical high-resolution mission for GMES operational services," Remote Sens. Environ., vol. 120, pp. 25–36, May 2012.
- [17] V. I. Feygels et al., "CZMIL (coastal zone mapping and imaging lidar): From first flights to first mission through system validation," Proc. SPIE Ocean Sens. Monitor., vol. 8724, Jun. 2013, Art. no. 87240A.
- [18] T. Neumann, A. Brenner, D. Hancock, J. Robbins, J. Saba, and K. Harbeck, "ICE, CLOUD, and Land Elevation Satellite-2 (ICESat-2) Project: Algorithm Theoretical Basis Document (ATBD) for Global Geolocated Photons: ATL03," Nat. Aeronaut. Space Admin., Greenbelt, MD, USA, Tech. Rep. Release 003, 2018. [Online]. Available: https://icesat-2.gsfc.nasa.gov/sites/default/files/page\_files/ICESat2\_ATL03\_ATBD\_r003.pdf
- [19] T. A. Neumann et al., "ATLAS/ICESat-2 L2A global geolocated photon data, version 1. [ATL03\_20181118073735\_07740106\_001\_01]," Nat. Snow Ice Data Center, Boulder, CO, USA, Tech. Rep., 2019. [Online]. Available: https://nsidc.org/data/atl03, doi: 10.5067/ATLAS/ATL03.001.
- [20] Z. Pan, C. Glennie, C. Legleiter, and B. Overstreet, "Estimation of water depths and turbidity from hyperspectral imagery using support vector regression," *IEEE Geosci. Remote Sens. Lett.*, vol. 12, no. 10, pp. 2165–2169, Oct. 2015.
- [21] D. R. Lyzenga, "Shallow-water bathymetry using combined lidar and passive multispectral scanner data," *Int. J. Remote Sens.*, vol. 6, no. 1, pp. 115–125, Jan. 1985.
- [22] Î. N. Figueiredo, L. Pinto, and G. Goncalves, "A modified Lyzenga's model for multispectral bathymetry using tikhonov regularization," *IEEE Geosci. Remote Sens. Lett.*, vol. 13, no. 1, pp. 53–57, Jan. 2016.
- [23] A. Misra, Z. Vojinovic, B. Ramakrishnan, A. Luijendijk, and R. Ranasinghe, "Shallow water bathymetry mapping using support vector machine (SVM) technique and multispectral imagery," *Int. J. Remote Sens.*, vol. 39, no. 13, pp. 4431–4450, Jul. 2018.
- [24] G. Shi, "Support vector machines," in Proc. Data Mining Knowl. Discovery Geoscientists, 2014, pp. 87–110.
- [25] N. Vladimir Vapnik, The Nature of Statistical Learning Theory. New York, NY, USA: Springer, 1999.
- [26] C.-C. Chang and C.-J. Lin, "LIBSVM," ACM Trans. Intell. Syst. Technol., vol. 2, no. 3, pp. 1–27, Apr. 2011.